Chemical Engineering Journal 500 (2024) 156711

Contents lists available at ScienceDirect

Chemical Engineering Journal

journal homepage: www.elsevier.com/locate/cej

Bacterial film-based degradable triboelectric nanogenerator for both contact and non-contact sensing

Baokun Zhang [a,b,1], Yang Zou [a,b,1,*], Minghao Liu [b,c], Engui Wang [b], Xi Cui [b], Yiqian Wang [b,c], Jiangtao Xue [a,b], Yujuan Li [a], Yulin Deng [a,*], Zhou Li [b,c,d,*]

[a] School of Medical Technology, Beijing Institute of Technology, Beijing 100081, China
[b] Beijing Institute of Nanoenergy and Nanosystems, Chinese Academy of Sciences, Beijing 101400, China
[c] Center on Nanoenergy Research, School of Physical Science and Technology, Guangxi University, Nanning, 530004, China
[d] School of Nanoscience and Engineering, University of Chinese Academy of Sciences, Beijing 100049, China

ARTICLE INFO

Keywords:
Bacterial film
Triboelectric nanogenerator
Contact sensing
Noncontact sensing
Degradable

ABSTRACT

As an emerging environmentally friendly energy conversion device, degradable triboelectric nanogenerators (TENGs) play an important role in self-powered sensing, health care and human–machine interaction. However, traditional degradable materials used in TENGs often suffer from limited material sources and complex preparation processes, restricting large-scale production for widespread applications. Here, we propose a simple and efficient way to prepare degradable TENGs with inactivated bacterial film, taking advantage of wide source, self-proliferation and easy culture properties of bacteria. The prepared bacterial film-based TENG (BF-TENG) has stable electrical output, good durability and fatigue resistance, along with superior capabilities in both contact and non-contact sensing. In contact mode, the BF-TENG can generate a peak voltage of up to 83.3 V, which is employed for accurate Morse code transmission. In non-contact mode, the BF-TENG is capable of effectively perceiving the target polymer at a distance of 150 cm. The non-contact LED control circuit and a sensing array based on BF-TENG further demonstrate its practical potential for gesture recognition and spatial position perception. Furthermore, the fully degradable nature of BF-TENG ensures effortless disposal after use without environmental impact, serving as a promising solution for the new generation of eco-friendly and sustainable sensing devices.

1. Introduction

The new generation of sensing technologies plays a crucial role in information transmission, human–machine interaction, and intelligent control[1–4]. Currently, most electronic products still rely on human operation, which includes both touch screen controls and contactless gesture controls. The combination of multiple control methods makes human–machine interaction more convenient, flexible, and diverse. Self-powered sensing technology based on triboelectric nanogenerators (TENGs) can effectively capture mechanical signals from the environment or human body without the need for external power sources [5–11]. Leveraging the triboelectric effect and electrostatic induction, TENGs can detect external mechanical signals through direct contact as well as perceive relative displacement and other states of objects in a non-contact manner[12]. Due to their high output, broad frequency response, and sensitivity to minute mechanical signals, TENGs are now widely used for tactile and pressure monitoring, vibration and acceleration detecting, sound sensing, physiological signal monitoring, human movement tracking, and motion energy harvesting[13–17].

The evolution of the electronics industry has been accompanied by the generation of substantial electronic waste, resulting in significant environmental challenges[18]. Recently, degradable devices that can naturally decompose after their lifecycle have rapidly attracted widespread interest and become an emerging research hotspot in materials science and electronics[19–22]. The wide material choices have facilitated the recent development of degradable TENGs, serving as transient electronics for applications in biomechanical energy harvesting and physiological signal sensing[23]. However, the current material sources for degradable TENGs mainly include animal-based, plant-based, and artificial synthesis, which are constrained by complex purification and

* Corresponding authors.
E-mail addresses: zouyang@bit.edu.cn (Y. Zou), deng@bit.edu.cn (Y. Deng), zli@binn.cas.cn (Z. Li).
[1] These authors contributed equally to this work.

https://doi.org/10.1016/j.cej.2024.156711

Available online 16 October 2024

film formation techniques, limiting the mass production of the devices [24–26]. Additionally, the relatively low electrical output performance also constrains their efficiency in practical use, especially in non-contact sensing applications[27–29].

Microorganisms are ubiquitous in nature and human society, playing a vital role in the fermentation industry[30,31], pharmaceutical production[32,33], and environmental remediation[34,35]. Biofilms formed by bacteria and their secretions represent a natural, degradable material with low production costs, self-proliferation, renewability, and pollution-free properties. Due to their intrinsic electron transfer capabilities, they can be developed into biosensors for environmental monitoring or utilized in biofuel cells for energy generation[36,37]. Recently, researchers have also designed a hydrovoltaic generator based on specific types of bacteria, capable of converting humidity from the environment into electrical energy[38–40]. The numerous outstanding characteristics of bacterial biofilms also position them as a promising naturally degradable material for fabricating biodegradable devices [41]. However, in the development of degradable TENGs, bacterial cellulose is frequently employed as a triboelectric material, while the direct use of bacterial biofilms to fabricate triboelectric devices is relatively uncommon[42–44].

Here, we utilized inactivated bacterial films as triboelectric material to develop a simple, rapid and efficient method for fabricating bacterial film-based TENG (BF-TENG). Three ubiquitous environmental bacteria, including Escherichia coli, Bacillus subtilis, and Staphylococcus aureus, were employed in the preparation of BF-TENG to explore their electricity generation performance. The influence of bacterial film thickness, dimensions, and ambient humidity on the output performance of BF-TENG was also investigated. Moreover, we found that the BF-TENG can serve as a self-powered sensing device, utilizing the triboelectric effect and electrostatic induction to enable both contact and contactless sensing. In the direct contact mode, an open-circuit voltage ranging from 4 V to as high as 85 V can be generated through contact separation with different polymer materials. Meanwhile, in the non-contact mode, BF-TENG is capable of sensing the target polymer at an ultra-long distance of up to 150 cm. The morse code signal transmission and non-contact LED switch control have been used to further demonstrate the dual operational modes of the BF-TENG. A 3 × 3 sensing array based on BF-TENG has also exhibited its potential for spatial positioning of objects and gesture recognition. Furthermore, the fully degradable nature of BF-TENG qualifies it as a sustainable, passive, and eco-friendly device, while its robust stability guarantees reliable output performance throughout its lifespan. The good degradability of the BF-TENG, coupled with its superior sensing capabilities in both contact and non-contact modes, positions it as an environmentally friendly electronic device with promising applications in human–machine interaction and intelligent control.

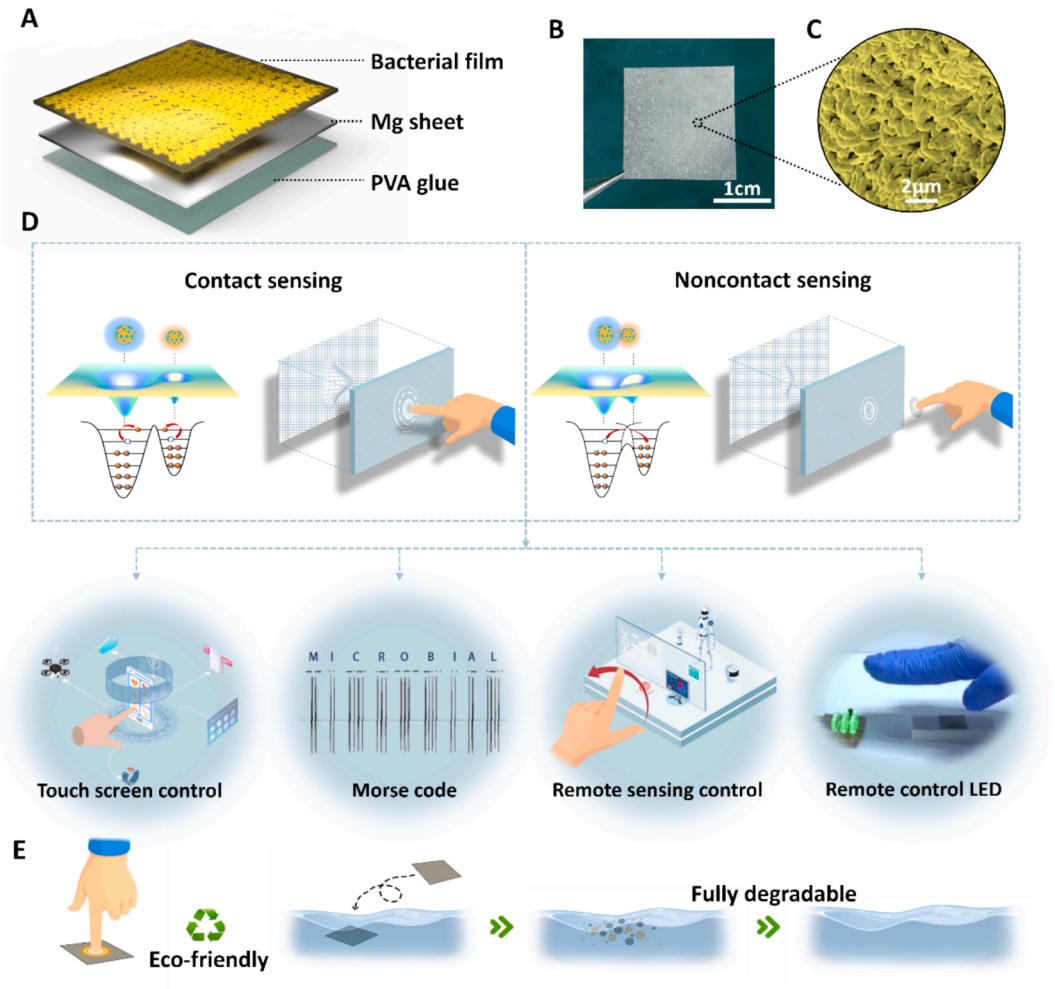

Fig. 1. (A) Schematic diagram of the 3D structure of BF-TENG. (B) Photograph of BF-TENG. (C) SEM image of the bacterial film of BF-TENG. (D) Illustration of the electron cloud model and potential applications of BF-TENG in contact and non-contact modes. (E) Illustration of the degradation process of BF-TENG in aqueous solution.

2. Results and discussion

2.1. Device composition and characteristics

Fig. 1A illustrates the schematic structure of the proposed bacterial film-based TENG (BF-TENG). Based on the single-electrode mode, the BF-TENG consists of a simple three-layer structure. Among them, the bacterial film acts as a triboelectric layer to directly sense the surface charge of the approaching object. The magnesium sheet underneath the bacterial film acts as an electrode layer to sense the charge variations on the bacterial film and generate induced charges. Due to magnesium being a reactive metal, the polyvinyl alcohol (PVA) glue layer at the bottom serves as a protective barrier, inhibiting the interaction between the magnesium sheet and the air to decelerate the oxidation of the magnesium electrode (Figure S1). The physical photo of BF-TENG is shown in Fig. 1B, and the scanning electron microscope (SEM) image of the device surface is shown in Fig. 1C. It can be seen that the surface of BF-TENG is covered with a dense layer of bacteria-formed film.

Fig. 1D displays the two working modes of BF-TENG as a sensor, showing simplified schematic diagrams for both contact sensing and non-contact sensing. The electron cloud model is employed to elucidate the electron transitions occurring in BF-TENG under its various operating modes. At the atomic level, the electron clouds of the interacting materials initially remain separate. However, under mechanical stress,

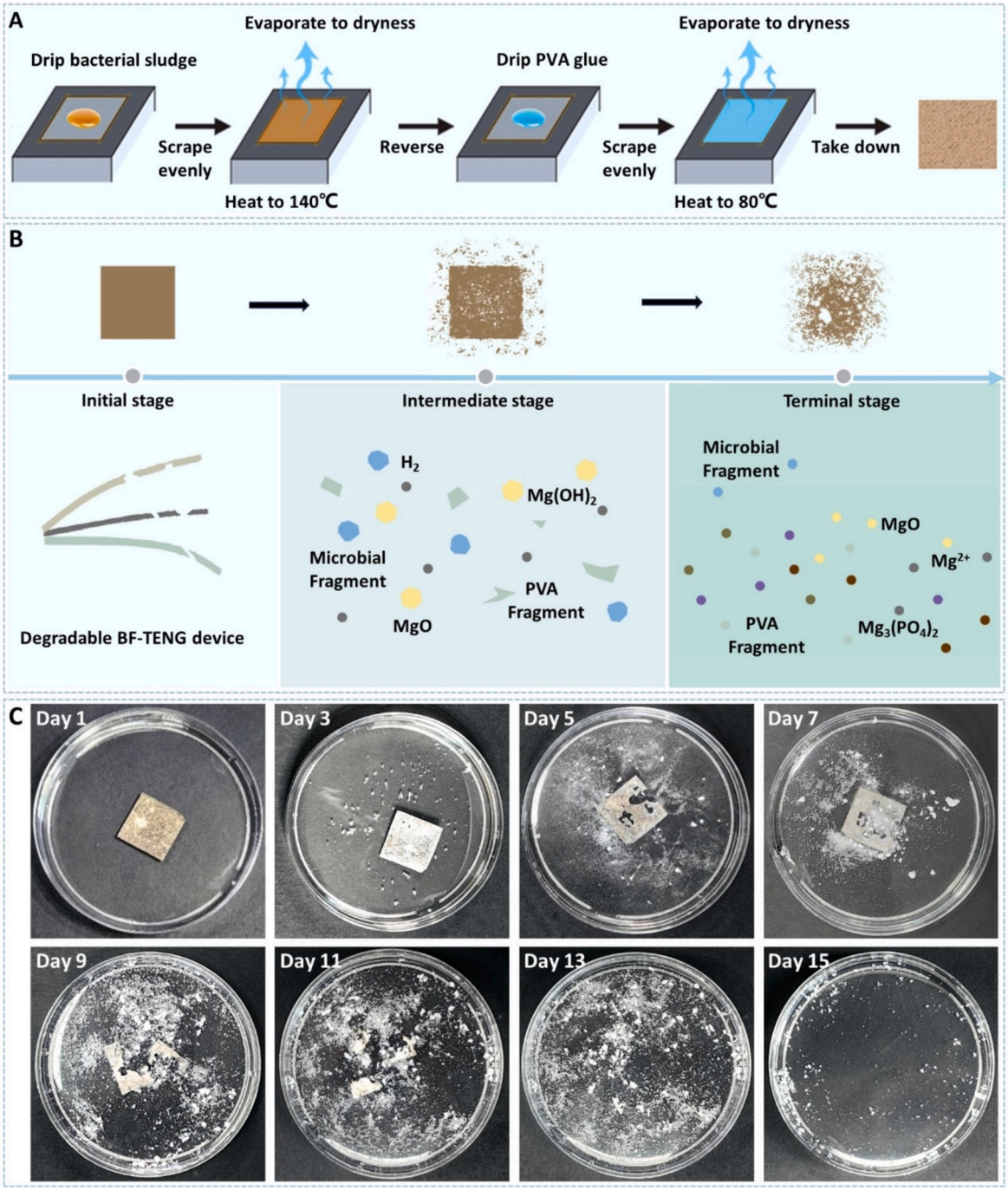

Fig. 2. (A) Schematic diagram of the preparation process of the BF-TENG. (B) Schematic diagram of the BF-TENG at different degradation stages and the corresponding products. (C) Actual photos of the BF-TENG degraded in 1 × PBS solution over 15 days.

these clouds begin to approach, guided by the principle that like charges repel and opposite charges attract, which governs electron movement. In contact sensing mode, the electron clouds in the BF-TENG model continue to move closer under mechanical influence until direct contact occurs. This interaction leads the clouds to overlap, diminishes the potential barrier, and facilitates electron transitions between the atoms. In non-contact sensing mode, as atoms draw near to the point of contact, two dense electron clouds position themselves adjacent to each other, initiating an internal charge directionally migration driven by electric field forces. In essence, reducing the distance between two atoms increases the overlap of their electron clouds, significantly lowering the potential barrier and enhancing the efficiency of electron transitions. The two operating modes endow BF-TENG with significant potential in various sensing domains, including touchscreen control, secure information transmission, human–machine interaction, and remote control of electronics. Moreover, the prepared BF-TENG is designed to be fully degradable, serving as an environmentally friendly device (Fig. 1E). After use or completing its service life, BF-TENG can be easily decomposed by simple treatment (immersion in solution) without causing any pollution to the environment.

2.2. Preparation of BF-TENG and characterization of bacterial film

Fig. 2A presents a schematic depiction of the process for creating BF-TENG devices. In the fabrication of BF-TENG, the preparation of a triboelectric layer based on bacterial film is essential. Here, a direct drying method is used to generate the bacterial film, which allows for convenient and rapid production, and the dimension and thickness of the bacterial film can also be controlled easily according to demand and dosage. Initially, the magnesium sheet was fixed to the surface of the heating stage using polyimide tape with a certain thickness. Subsequently, the centrifuged bacterial sludge was dropped onto the center of the magnesium sheet and spread evenly by a scraper. The heating stage was preheated to 140 °C to evaporate and dry the bacterial sludge into a film. Moreover, the established heating and drying temperature can effectively achieve bacterial inactivation, thereby eliminating the risk of bacterial infection when the device is in use[45]. After heating for a period of time (15 min), a film composed of inactivated bacteria formed on the surface of the magnesium sheet. Then, the magnesium sheet covered with the bacterial film was turned over and fixed on the heating stage again. PVA glue was dripped on the other surface of the magnesium sheet and scraped evenly, and then dried to form a film by heating it to 80 °C on the heating stage. Finally, the tape was removed and the magnesium sheet covered with the bacterial film and PVA film was taken down, completing the fabrication of a BF-TENG.

In order to investigate the film-forming characteristics of various bacterial species and assess their efficacy in constructing TENGs, three kinds of bacteria commonly found in nature, Escherichia coli (E.coli), Staphylococcus aureus (S.aureus) and Bacillus subtilis (B.subtilis), were selected for research. E.coli is a resident bacterium in the gastrointestinal tracts of humans and animals, which is characterized by rod-shaped morphology. S.aureus is frequently present on human skin and mucous membranes, distinguished by round, grape-like clustering. B. subtilis, a commonly found soil bacterium, is also used as a probiotic for temporary colonization of the gastrointestinal tract, with a rod-shaped morphology but smaller compared to E.coli. Figure S2 provides illustrations of the primary structural morphology of the three bacterial species.

Based on the method mentioned above, films of these three bacteria were prepared on the surface of magnesium sheets, respectively. The SEM images of the surface of the three bacterial films are shown in Figure S3 (magnified 5000 times), all three bacteria formed uniform and continuous films, demonstrating the general applicability of this method for film formation on different bacteria. The higher magnification SEM images (magnified 10,000 times) reveal that the three bacteria films were formed by a large number of stacked bacteria with intact morphology and distinct characteristics, respectively. The thickness of the bacterial film can be regulated by controlling the dose of the bacterial sludge. Figure S4 shows the cross-sectional SEM images of E.coli films with different thicknesses (approximately 3 μm, 6 μm and 9 μm), which were prepared from 200 μL, 400 μL, and 600 μL of centrifuged bacterial sludge, respectively. The atomic force microscopy images of the E.coli film surface are shown in Figure S5, which shows that the heights across different regions of the bacterial film surface are relatively consistent. Energy dispersive spectrometer (EDS) measurement was used to analyze the distribution of major elements on the surface of bacterial films. Figure S6 shows the distribution of carbon, nitrogen, and oxygen elements on the surface of the film formed by E. coli, further proving the homogeneity of the bacterial film structure. The Fourier Transform Infrared Spectroscopy (FTIR) testing was also performed on the surface of the E. coli film, which shows the absorption peaks of various functional groups on the surface of the bacterial film (Figure S7). Furthermore, after 100 continuous bending tests, the bacterial film on the surface of the BF-TENG showed no signs of peeling (Figure S8), demonstrating the good adhesion of the bacterial film, which meets the requirements for practical applications.

2.3. Degradability of BF-TENG

Since the bacterial film, magnesium electrode and PVA glue used in the preparation of BF-TENG can be degraded, the prepared BF-TENG also exhibits good degradation performance and can be easily decomposed after use without causing pollution to the environment. By continuously observing the degradation state of BF-TENG over time, we further investigated the degradability of BF-TENG. To eliminate the impact of pH changes on the degradation process, phosphate-buffered saline (PBS) was chosen for the degradation test to provide a relatively stable pH environment. A prepared BF-TENG with the size of 2 cm × 2 cm was placed in a petri dish containing 1 × PBS solution, and the degradation experiment was performed at 37 °C in a constant temperature incubator. Observations were conducted every 24 h to track the degradation process. Fig. 2B illustrates the schematic of the degradation process of BF-TENG at different stages. Fig. 2C and Figure S9 show the optical photos of the degradation state of BF-TENG over a period of 15 consecutive days. It can be observed that, during the initial 1–3 days, the bacterial film peels off from the magnesium electrode and breaks down into small fragments, which are subsequently dispersed in the solution. Simultaneously, the PVA glue layer on the back of the magnesium electrode rapidly dissolves in the solution. When the magnesium electrode surface is exposed to the solution, the generation of bubbles is observed, indicating a reaction between magnesium and water to produce hydrogen gas and magnesium hydroxide. In the subsequent stage, the degree of degradation of the device mainly depends on the corrosion of the magnesium sheet, which gradually expands from local pitting to a large area of defect. By the 13th day, there is almost no intact magnesium sheet visible, indicating that the magnesium electrode has completely become into corrosion products such as magnesium oxide, magnesium hydroxide, and magnesium phosphate. By the 15th day, only a small amount of precipitate can be observed, which indicates that in the terminal degradation stage, the corrosion products continue to dissolve in the solution and form a small amount of insoluble precipitate. The mass variation of BF-TENG in 1 × PBS solution is shown in Figure S10, which further proves the well degradation rate of the device. In addition, the degradation behavior of the BF-TENG in soil further demonstrated the degradability of the bacterial film in the natural environment as well as the recyclability of the magnesium sheet (Figure S11). The above degradation process proves that BF-TENG has the potential as a transient electronic device, capable of rapidly decomposing in solution after use.

2.4. Electrical output performance of BF-TENG

Fig. 3A illustrates the working principle of BF-TENG with contact-separation mode during one operating cycle. In the initial state, the BF-TENG comes in contact with an external contact material, and equivalent and opposite charges are generated on the surfaces of the bacterial film and the contact material due to the triboelectrification effect. When the BF-TENG is separated from the contact material, the equilibrium state is broken, and the magnesium electrode is induced by electrostatic induction to carry the corresponding charge. To re-attain equilibrium, electrons on the magnesium electrode flow towards the ground through an external circuit, thereby generating an electrical output signal. The electrical output is maximized when the BF-TENG is completely separated from the contact material and reaches a sufficient distance. When the BF-TENG approaches the contact material again, electrons flow back from the ground to the magnesium electrode via an external circuit, producing an opposite electrical output signal. When the bacterial film is in full contact with the contact material, BF-TENG returns to the initial state and starts a new working cycle.

The electrical output performance of BF-TENG was characterized by an electrometer and an oscilloscope. A linear motor was used to control the contact and separation of the contact material from the BF-TENG and provide periodic motion. A 5 cm × 5 cm acrylic sheet was fixed on the linear motor as a contact material platform. In order to investigate the effect of the films formed by different bacterial species on the construction of BF-TENG, different bacterial films with the same thickness (about 3 μm) and size (2 cm × 2 cm) were prepared into BF-TENGs for testing. The open-circuit voltage (V_{oc}), short-circuit current (I_{sc}) and transferred charge (Q_{sc}) of BF-TENG prepared from films of E.coli, S. aureus and B.subtilis are shown in Fig. 3B-D, respectively. The results indicate that BF-TENGs constructed from all three bacterial films exhibit stable electrical output signals. Compared to the BF-TENGs constructed with the other two bacterial films, the BF-TENG made with the E. coli film shows a higher output with a V_{oc} of about 5.2 V, an I_{sc} of about 50.5nA, and a Q_{sc} of about 2.0 nC. In addition, considering that E.coli is easy to culture and purify with low pathogenicity, BF-TENG prepared by

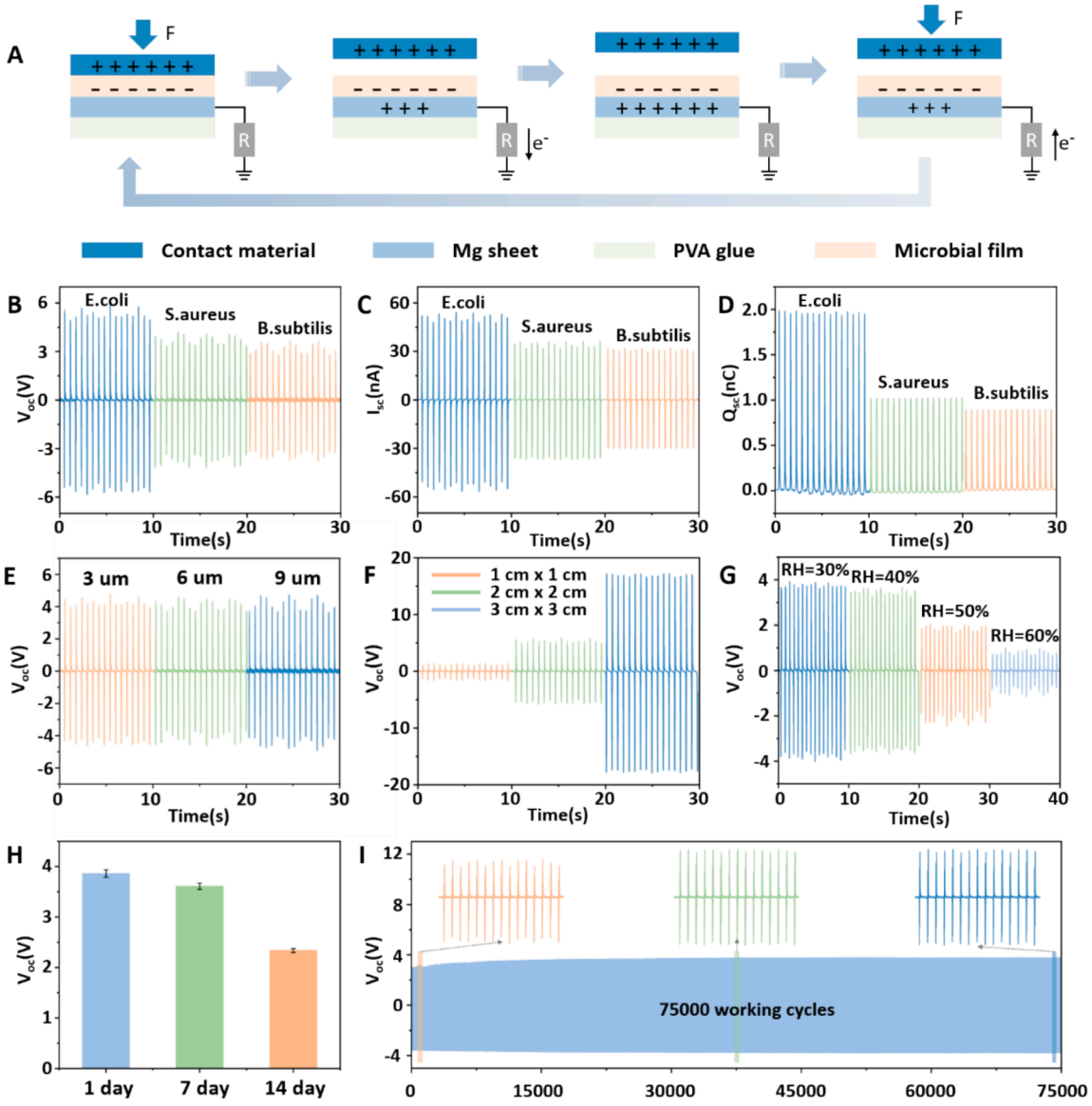

Fig. 3. (A) Schematic diagram of the contact sensing principle of BF-TENG. (B-D) The output open-circuit voltage (V_{oc}), short-circuit current (I_{sc}) and transferred charge (Q_{sc}) of BF-TENG prepared by three kinds of bacterial film (E.coli, S.aureus and B.subtilis). (E) The output V_{oc} of BF-TENG prepared with E. coli films of three different thicknesses (3 μm, 6 μm, 9 μm). (F) The output V_{oc} of BF-TENG prepared with E. coli films of three different sizes. (G) The output V_{oc} of BF-TENG under different relative humidities (from 30 % to 60 %). (H) The output V_{oc} of BF-TENG in durability test. (I) The output V_{oc} of BF-TENG in continuous fatigue test.

E.coli film was used for all subsequent experiments. Here, we further investigated the impact of bacterial film thickness and size on the output of the BF-TENG. As shown in Fig. 3E, the BF-TENGs constructed with bacterial films of approximately 3 μm, 6 μm, and 9 μm thickness (with the same size of 2 cm × 2 cm) have similar output open-circuit voltages, indicating that the thickness of bacterial film has no significant effect on the output of BF-TENGs. The output V_{oc} of BF-TENG prepared from bacterial films with the same thickness (3 μm) and different sizes (1 cm × 1 cm, 2 cm × 2 cm, and 3 cm × 3 cm) is shown in Fig. 3F, and the corresponding I_{sc} and Q_{sc} are shown in Figure S12. The results show that as the size of the device increases, the output of the BF-TENG significantly improves. This is due to the larger size implying a greater contact area, which leads to the generation of more contact charges, thereby enhancing the electrical output performance of BF-TENG.

The influence of ambient humidity on the output of BF-TENG was further investigated. When the relative humidity (RH) increased from 30 % to 60 %, the V_{oc} of the BF-TENG output decreased from 3.8 V to 0.8 V (Fig. 3G), the I_{sc} decreased from 26.5nA to 1.5nA, and the Q_{sc} decreased from 1.8nC to 0.1nC (Figure S13). This is because as the humidity increases, more small droplets are generated in the environment, which neutralizes the electrostatic charge on the BF-TENG surface, reduces the electrostatic field, and ultimately leads to a decrease in the output of the BF-TENG. To verify that the output attenuation of BF-TENG due to ambient humidity is reversible, we also tested the output voltage of BF-TENG under ambient humidity (30 % RH), after being placed in 60 % RH for 1 h, and then after being placed back in the ambient humidity (30 % RH) for another hour (Figure S14). The results indicate that the output of BF-TENG can be effectively restored by placing the device back in dry conditions.

The electrical output of the BF-TENG under different contact-separation frequencies was also measured. As shown in Figure S15, with the increase of working frequency, the output V_{oc} and I_{sc} of BF-TENG increase, while the change of Q_{sc} is relatively small. To verify the durability of the BF-TENG, the output V_{oc} of the prepared BF-TENG

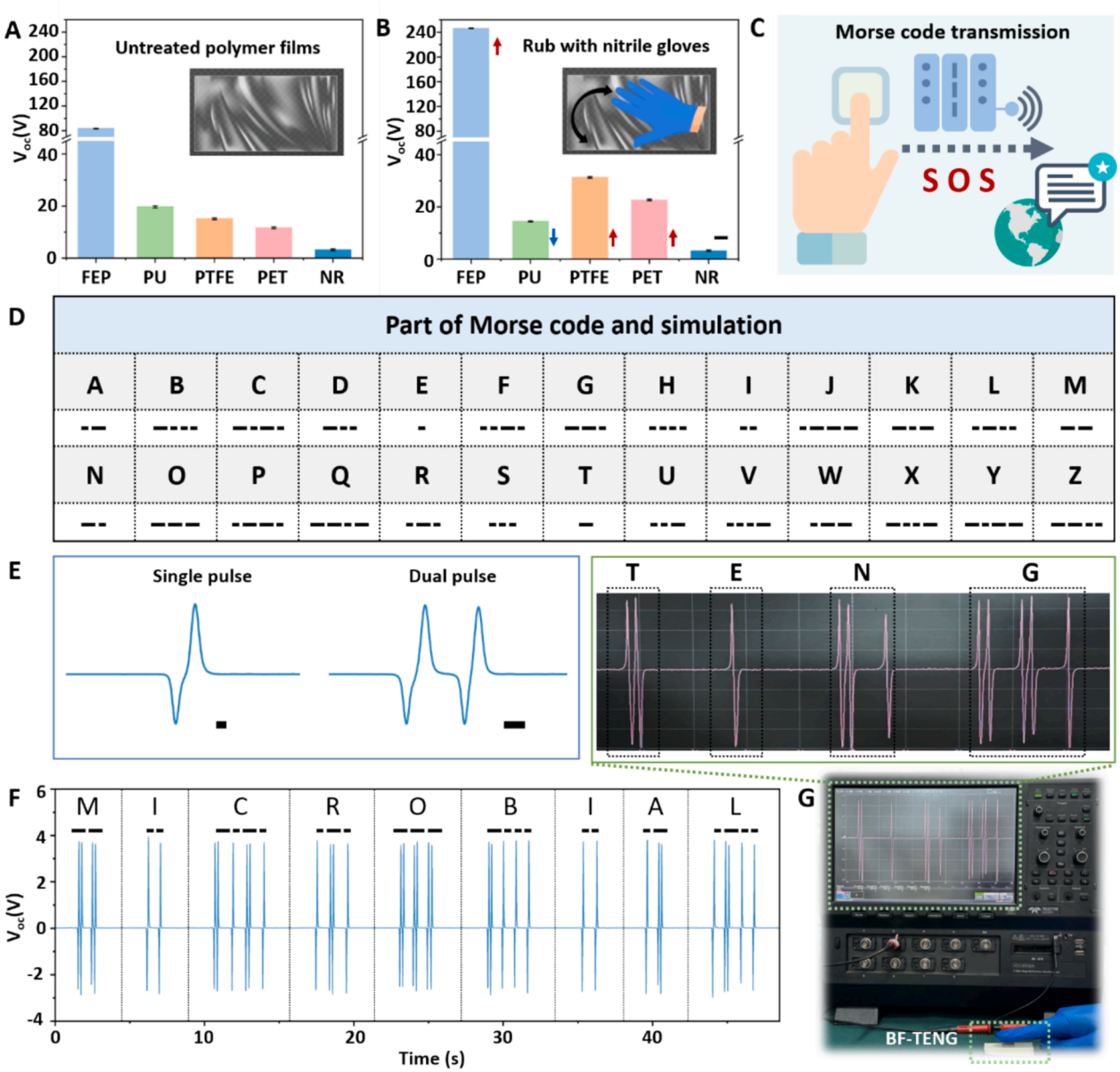

Fig. 4. (A) The output V_{oc} of BF-TENG in contact and separation with five different polymers. (B) The output V_{oc} of BF-TENG in contact and separation with five different polymers after rubbing with nitrile gloves. (C) Illustration of BF-TENG used for Morse code transmission. (D) Part of Morse code and simulation. (E) A short dot signal (dit) and a longer dash signal (dah) represented by single pulse and dual pulse of BF-TENG, respectively. (F) String information of "MICROBIAL" transmitted by BF-TENG. (G) Actual photo of string information of "TENG" transmitted by BF-TENG.

was measured on the 1st day, the 7th day, and the 14th day under the storage conditions of indoor temperature and humidity environment, respectively (Fig. 3H). The results showed that the output V_{oc} of the BF-TENG decreased only slightly from 3.9 V to 3.6 V during the first week, and after two weeks, the V_{oc} of the BF-TENG decreased to about 2.3 V. Furthermore, after undergoing 75,000 continuous working cycles (at a working frequency of 1.5 Hz), the output V_{oc} of the BF-TENG showed almost no attenuation, demonstrating its superior fatigue resistance and output stability (Fig. 3I).

2.5. Contact sensing and application of BF-TENG

Based on the working principle of triboelectric nanogenerators, the triboelectric effect will exist in any two materials during contact separation. Therefore, BF-TENG can be used as a contact sensor to detect external objects. Here, we explored the output V_{oc} of BF-TENG in contact with five common polymer materials, including fluorinated ethylene propylene (FEP), polytetrafluoroethylene (PTFE), polyurethane (PU), polyethylene terephthalate (PET), and nitrile rubber (NR). Each polymer film with a size of 5 cm × 5 cm was fixed on a linear motor platform to contact with BF-TENG. As shown in Fig. 4A, the BF-TENG exhibited different V_{oc} when it came into contact and separated with different polymer films. When in contact with FEP, the BF-TENG can generate a V_{oc} as high as 83.3 V, whereas when in contact with NR, it only produces a V_{oc} of 3.2 V. This is due to the different electron affinity of different materials. FEP has a strong ability to obtain electrons, and it is easy to be negatively charged when in contact with the bacterial film of BF-TENG, while the electron affinity of NR is similar to that of bacterial film, resulting in a smaller potential difference between the two. The output voltage, current and power density of BF-TENG (FEP as the contact material) with a series of loading resistances are shown in Figure S16. When the load is 100 MΩ, the BF-TENG achieves a maximum output power density of about 60 mW/m^2, which indicates that the internal impedance of the BF-TENG is around 100 MΩ.

It is worth mentioning that the BF-TENG is also capable of sensitively detecting the charge state of external objects. When rubbing different polymer films with nitrile gloves, a certain amount of charge will accumulate on the surface of the polymer film in advance. When BF-TENG came into contact with these polymer films again, the output V_{oc} changed significantly. The results of Fig. 4B show that the V_{oc} caused by the FEP film after rubbing with nitrile gloves increased from 83.3 V to 246.3 V, the V_{oc} for the PTFE film increased from 15.1 V to 31.3 V, the V_{oc} for the PET film increased from 11.6 V to 22.7 V, while the V_{oc} for the PU film decreased from 19.7 V to 14.5 V and the V_{oc} for the NR film remained almost unchanged. Based on previous research, it is known that PET, PTFE and FEP are more likely to obtain electrons than NR, while PU is more likely to lose electrons than NR[46]. Therefore, when these materials rub with nitrile gloves, electrons will be transferred to materials that are easier to obtain electrons, thereby changing the charge on the surface of the contact material and further affecting the output voltage. Here, according to the changing trend of the corresponding output V_{oc} of BF-TENG, we can infer that the triboelectric sequence of the bacterial film is located between NR and PET, which can effectively sense the charged state of various materials.

Due to its good contact sensing properties, the BF-TENG can be used for signaling applications. Morse code is a kind of on–off signal code that expresses different information through specific sequences. Due to its simplicity, ease of learning and use, despite the highly advanced state of modern communication technologies, Morse code continues to serve in certain specialized fields and situations, such as instant encrypted communications and emergency distress signals. BF-TENG can generate electrical signals through contact with a wide range of external objects without the need for an additional power supply. The direct control of electrical signal output through physical contact aligns well with the format of Morse code. Here, we demonstrated the potential of BF-TENG for encoding signals and transmitting Morse code information (Fig. 4C). Morse code utilizes two fundamental signals: a short dot signal (dit) and a longer dash signal (dah) to represent different characters. Fig. 4D illustrates the representation of 26 English letters in Morse code. By interacting with the BF-TENG, the generation of single and dual pulse signals can be controlled, corresponding to the dot and the dash signals in Morse code, respectively (Fig. 4E). As shown in Fig. 4F and G, the information of 'MICROBIAL' and 'TENG' can be clearly expressed and displayed by the continuous pulse signal output by BF-TENG.

2.6. Non-contact sensing and application of BF-TENG

During the test, we noticed that when the external object was not in direct contact with the BF-TENG, only changing the distance between the two led to electrical signals generated by BF-TENG, which indicated that the BF-TENG could also operate in a non-contact mode. Here, we further explored the non-contact sensing capabilities of the BF-TENG and its corresponding applications. The working principle of non-contact sensing for BF-TENG is illustrated in Fig. 5A. When the sensing object is close to BF-TENG, the electric field will be redistributed due to the electrostatic induction. Taking nitrile gloves as an example, when the nitrile gloves are close to the bacterial film layer on the surface of BF-TENG, the potential difference between the magnesium electrode layer and the ground will cause electron flow, resulting in an electrical signal. When the nitrile gloves are separated from BF-TENG, electrons flow back from the electrode layer to the ground, resulting in a reverse electrical signal.

To investigate the effective distance of a target object that can be sensed by the BF-TENG in non-contact mode, the BF-TENG was fixed on an insulating plate (polylactic acid plate made by 3D printing) facing the detection target, as shown in Fig. 5B. When the hand-held FEP roll (40 × 20 cm^2 with a thickness of 0.1 mm) was shaken at a distance of 50 cm, 100 cm and 150 cm from BF-TENG, the corresponding open-circuit voltage (Fig. 5C and Supplementary Video 1), short-circuit current (Figure S17A) and transferred charge (Figure S17B) of BF-TENG were measured. It can be seen from the results that when the distance is 50 cm, BF-TENG can produce a high electrical output to sense the movement of the target FEP roll, with a V_{oc} of 4.7 V, I_{sc} of 307.7nA and Q_{sc} of 8.7 nC. As the distance increases, the output of BF-TENG decreases significantly. However, the BF-TENG can still produce stable electrical signals even at a distance as far as 150 cm, with a V_{oc} of 0.12 V, I_{sc} of 10.0nA and Q_{sc} of 0.4 nC, demonstrating its long-distance sensing capability for specific target polymer. Additionally, the response times of the BF-TENG in both working modes at a frequency of 50 Hz were also tested. As shown in Figure S18, the response time in contact mode is 1.45 ms, while in non-contact mode it is 4.37 ms. The fast response time makes the BF-TENG suitable for effective capturing of dynamic environmental signals. It is well known that the output of TENGs is directly related to the contact area[47,48]. The bacterial film in the BF-TENG contains a large number of natural micro-nano structures on its surface, which results in a larger surface area for the sensing device. When in contact with or close to external objects, it can generate or induce more surface charges, thereby exhibiting superior sensing performance in both working modes.

BF-TENG can also respond to different gestures in non-contact mode. Fig. 5D-E show the output V_{oc} generated by the BF-TENG when three gestures were performed above the BF-TENG surface, including slowly dropping and rapidly lifting a finger, rapidly dropping and slowly lifting a finger, making a fist and opening the palm, respectively. From the results, it can be observed that the V_{oc} waveforms generated by the BF-TENG are opposite when the finger was dropped after lifting and the palm was opened after holding the fist. At the same time, the speed of the finger dropping or lifting can also be distinguished by the peak voltage. A faster speed will lead to a higher peak voltage. Utilizing the non-contact sensing capacity of the BF-TENG, here we constructed a non-contact LED control circuit based on the BF-TENG (Fig. 5G). When the palm approaches the BF-TENG, the BF-TENG will generate an

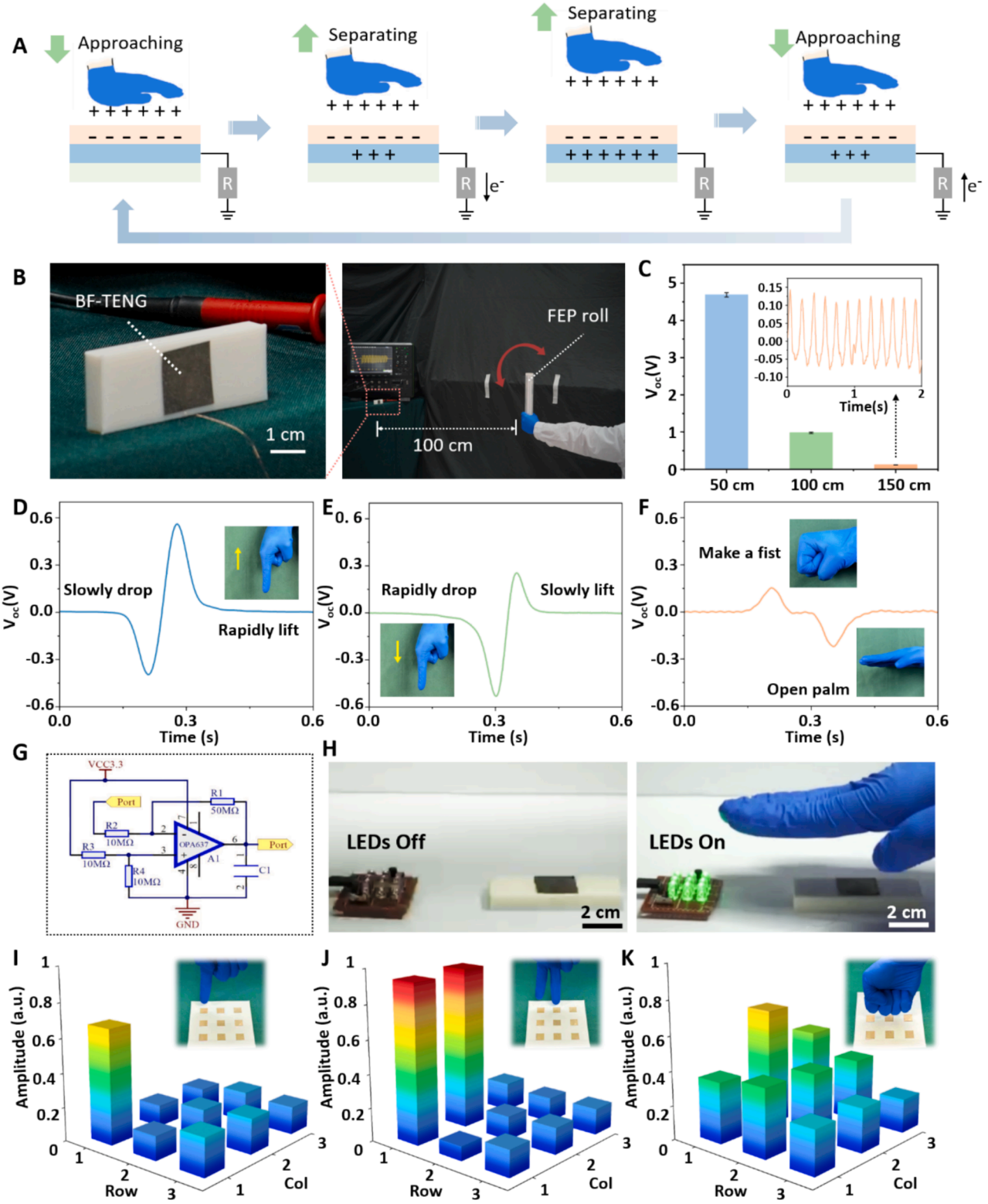

Fig. 5. (A) Schematic diagram of the non-contact sensing principle of BF-TENG. (B) Actual photos of BF-TENG for non-contact sensing testing. (C) The output V_{oc} of BF-TENG sensing the target polymer at 50 cm, 100 cm, and 150 cm distances. (D-F) The V_{oc} signal output by BF-TENG when sensing three different gestures. (G) The circuit diagram for using BF-TENG to control LEDs in a non-contact manner. (H) Actual photos of non-contact control of LEDs using BF-TENG. (I-K) A 3 × 3 sensor array based on BF-TENG used for spatial positioning of three gestures.

electrical signal that exceeds the set threshold voltage, thereby realizing the switching of the LED on/off state, as shown in Fig. 5H and Supplementary Video 2.

To achieve the perception of the spatial position of the object, a 3 × 3 sensing array based on BF-TENG was further constructed. By simultaneously measuring the output signals of nine sensors and displaying their corresponding peak voltages in the form of a visual 3D array diagram, the spatial position of the object can be effectively identified

(Fig. 5I-K). When the finger or fist approaches the sensing array, only the sensor at the corresponding position will have an obvious electrical signal response, which proves the good spatial perception ability of the BF-TENG sensing array. The above results indicate that the BF-TENG exhibits excellent non-contact sensing performance, showing great potential in long-distance specific object perception, gesture recognition, circuit control, and spatial object positioning.

3. Conclusions

In this study, we proposed a degradable triboelectric nanogenerator with bacterial film as the core component, which exhibits superior contact sensing and non-contact sensing capabilities. BF-TENG constructed from various types of bacteria exhibited stable electrical output. The performance of BF-TENG remained nearly constant after 75,000 consecutive working cycles and showed only slight attenuation after 14 days under indoor conditions, demonstrating its excellent fatigue resistance and durability. In contact working mode, BF-TENG can generate a V_{oc} ranging from 3.2 V to as high as 83.3 V when interacting with different polymer films. In non-contact working mode, BF-TENG can effectively sense the movement of the FEP roll within a range of 150 cm. Morse code message transmission and non-contact LED control have further showcased the practical contact and non-contact sensing capabilities of the BF-TENG. A 3 × 3 sensing array has also demonstrated its potential for spatial position perception of objects and gesture recognition. Beyond these applications, BF-TENG also holds promise for robotic tactile and perception in the future. Since BF-TENG exhibits significant electrical output differences for various contact polymers, it is also expected to be used for material or object recognition when combined with emerging artificial intelligence.

Additionally, BF-TENG presents good degradability, virtually disappearing in 1 × PBS solution within 15 days without other treatment. Leveraging the abundant sources and self-proliferation characteristics of bacteria, BF-TENG can be easily and rapidly prepared in batches, serving as an eco-friendly electronic device with significant potential in new-generation sensing technology. By comparing with some of the latest degradable TENG devices (Table S1), the BF-TENG demonstrates advantages such as wide material availability, ease of fabrication, and low cost, while also exhibiting good electrical performance and degradability. The dual working modes further significantly expand its potential applications.

Although BF-TENG has significant advantages in terms of dual-mode sensing performance, degradability, and material sources, it still faces some challenges in practical applications. For instance, environmental humidity significantly affects the device's output performance. Future research could focus on designing unique packaging materials and structures that enhance the device's resistance to environmental humidity without compromising its electrical performance, thereby making BF-TENG suitable for more complex working environments. Additionally, current BF-TENG exhibits extremely high output performance only with specific polymers (such as FEP). Enhancing its general output capability for a wider range of contact and sensing materials is another important direction for future improvements. Surface modification methods, such as chemical modification of bacterial films, could be considered to further enhance charge carrying capacity and thereby improve electrical performance.

4. Experimental

4.1. Bacteria culture

Escherichia coli, Staphylococcus aureus, and Bacillus subtilis were selected as experimental materials. Since there was no significant difference in the culture conditions of the three bacteria, they were all cultured with Luria-Bertani Broth at 37 °C in a CO_2 incubator. Following this, the cultured bacterial solutions were streaked onto agar plates using a three-zone streaking method within a biosafety cabinet. The plates were then incubated for 24 h in the CO_2 incubator. After incubation, single colonies were selected and re-cultured in liquid medium for further amplification. Due to the different reproduction rates of the three bacteria, the incubation times for them in this study were also different. The OD value reading was used as the standard for ending incubation to obtain bacterial suspensions of the same concentration. At an absorbance of 600 nm, the OD value of the bacterial suspension minus the OD value of the blank control medium should be 0.3. Finally, 4 ml of the cultured bacterial suspension was transferred to a sterile centrifuge tube and centrifuged at 5000 rpm for 5 min. The supernatant was discarded, and the bacterial sludge was collected.

4.2. Characterization and measurement of BF-TENG

The electrometer (Keithley 6517B) and oscilloscope (Teledyne LeCroy HD 4096) were used to measure the open-circuit voltage, short-circuit current and transferred charge of BF-TENG. A scanning electron microscope (Nova nanoSEM 450) with an Energy dispersive X-ray Spectroscopy (EDS) module was used to observe the microscopic morphology and the micro-regional energy spectral composition of bacterial film. A linear motor (LinMot E1100) was used to provide periodic motion for testing the output performance of BF-TENG. By adjusting the maximum speed and acceleration of the linear motor, different operating frequencies can be set.

Supplementary material.

Comparison of the magnesium electrode before and after natural oxidation with and without PVA encapsulation. Schematic diagram of the structural morphology of Escherichia coli (E.coli), Staphylococcus aureus (S.aureus) and Bacillus subtilis (B.subtilis). SEM images of the bacterial film of E.coli, S.aureus and B.subtilis (5000 × magnification) and higher magnification SEM images of E.coli, S.aureus and B.subtilis (10000 × magnification). Cross-sectional SEM images of the prepared E. coli films with different thicknesses (3 μm, 6 μm, 9 μm). Atomic force microscopy images of different regions of the E. coli film surface. Micro-regional energy spectral composition of E.coli film, including carbon, nitrogen and oxygen elements. Fourier Transform Infrared Spectroscopy (FTIR) of the E. coli film surface. Comparison of bacterial film on the upper surface of BF-TENG before and after bending 100 times. Actual photos of the BF-TENG degraded in 1 × PBS solution for 15 consecutive days. Mass variation of BF-TENG in phosphate-buffered saline. Degradation behavior of BF-TENG in soil for seven days. The output I_{sc} and Q_{sc} of BF-TENG prepared with E. coli films of three different sizes. The output I_{sc} and Q_{sc} of BF-TENG under different relative humidities (from 30 % to 60 %). Comparison of the output voltage of BF-TENG before and after being placed for 1 h at 60 % RH and 30 % RH conditions. The output Voc, Isc and Qsc of BF-TENG under different contact-separation frequencies (from 1 Hz to 5 Hz). Output voltage, current and power density of BF-TENG with various loading resistances. The output I_{sc} and Q_{sc} of BF-TENG sensing the target polymer at 50 cm, 100 cm, and 150 cm distances. Response time of BF-TENG in two working modes. Comparison of BF-TENG with other degradable TENG devices.

CRediT authorship contribution statement

Baokun Zhang: Writing – original draft, Visualization, Methodology, Investigation, Formal analysis, Data curation, Conceptualization. **Yang Zou:** Writing – review & editing, Visualization, Project administration, Methodology, Investigation, Funding acquisition, Conceptualization. **Minghao Liu:** Visualization, Software, Methodology, Investigation. **Engui Wang:** Visualization, Methodology, Investigation, Formal analysis. **Xi Cui:** Visualization, Investigation, Formal analysis. **Yiqian Wang:** Visualization, Methodology, Investigation. **Jiangtao Xue:** Visualization, Methodology, Formal analysis. **Yujuan Li:** Resources, Methodology. **Yulin Deng:** Writing – review & editing, Validation, Supervision, Resources, Project administration,

Conceptualization. **Zhou Li:** Writing – review & editing, Supervision, Project administration, Funding acquisition, Conceptualization.

Declaration of competing interest

The authors declare that they have no known competing financial interests or personal relationships that could have appeared to influence the work reported in this paper.

Acknowledgments

This study was supported by the National Natural Science Foundation of China (T2125003, 82202075), Beijing Natural Science Foundation (L212010), the National Postdoctoral Program for Innovative Talent (BX20220380), China Postdoctoral Science Foundation (2022M710389), and the Fundamental Research Funds for the Central Universities. The authors thank everyone who helped in this work.

Appendix A. Supplementary data

Supplementary data to this article can be found online at https://doi.org/10.1016/j.cej.2024.156711.

Data availability

Data will be made available on request.

References

[1] Y.L. Yun, D.X. Ma, M.H. Yang, Human-computer interaction-based Decision Support System with Applications in Data Mining, Future Generation Computer Systems-the International Journal of Escience 114 (2021) 285–289.
[2] Y.J. Tang, et al., Triboelectric Touch-Free Screen Sensor for Noncontact Gesture Recognizing, Advanced Functional Materials 30 (5) (2020).
[3] R.Y. Liu, et al., Ultrathin, transparent, and robust self-healing electronic skins for tactile and non-contact sensing, Nano Energy 95 (2022).
[4] Y. Xi, et al., Self-powered wearable IoT sensors as human-machine interfaces, Soft Science 3 (3) (2023) 26.
[5] F.R. Fan, Z.Q. Tian, Z.L. Wang, Flexible triboelectric generator!, Nano Energy 1 (2) (2012) 328–334.
[6] H. Wu, et al., *Achieving ultrahigh instantaneous power density of 10 MW/m by leveraging the opposite-charge-enhanced transistor-like triboelectric nanogenerator (OCT-TENG).* Nature, Communications 12 (1) (2021).
[7] Z.Y. Zhu, et al., Self-powered silicon PIN neutron detector based on triboelectric nanogenerator, Nano Energy 102 (2022).
[8] C. Xu, et al., Portable and wearable self-powered systems based on emerging energy harvesting technology, Microsystems & Nanoengineering 7 (1) (2021) 25.
[9] Q. Du, et al., Physical Biomedical Science: A New Field of Original Interdisciplinary Research, Chin. Sci. Bull. 69 (2024) 2008–2014.
[10] Y. Mao, et al., Extraordinary-durable cylindrical rotary triboelectric nanogenerator based on CB/Fe3O4/PDMS microarrays for energy harvester, Nano Energy 125 (2024).
[11] Y. Mao, et al., Triboelectric nanogenerator/supercapacitor in-one self-powered textile based on PTFE yarn wrapped PDMS/MnO2NW hybrid elastomer, Nano Energy 84 (2021).
[12] X.F. Fu, et al., Non-Contact Triboelectric Nanogenerator, Advanced Functional Materials 33 (2023) 52.
[13] K.B. Chang, et al., A triboelectric nanogenerator-based tactile sensor array system for monitoring pressure distribution inside prosthetic limb, Nano Energy 111 (2023).
[14] X.M. Huo, A self-powered triboelectric pressure sensor for basketball training monitoring, Materials Letters 320 (2022).
[15] W. Ou-Yang, et al., Recent advances in triboelectric nanogenerator-based self-powered sensors for monitoring human body signals, Nano Energy 120 (2024).
[16] T. Song, et al., A strategy for human safety monitoring in high-temperature environments by 3D-printed heat-resistant TENG sensors, Chemical Engineering Journal 475 (2023).
[17] L. Liu, et al., Hybrid tribo/piezoelectric nanogenerator textile derived from 3D interlocked parallel-arranged yarns for bio-motion energy harvesting and tactile sensing, Chemical Engineering Journal 474 (2023).
[18] Andeobu, L., S. Wibowo, and S. Grandhi, An assessment of e-waste generation and environmental management of selected countries in Africa, Europe and North America: A systematic review. Science of the Total Environment, 2021. **792**.
[19] A. Baburaj, et al., Biodegradable based TENGs for self-sustaining implantable medical devices, Nano Energy 127 (2024).
[20] S.-W. Hwang, et al., A Physically Transient Form of Silicon Electronics, Science 337 (6102) (2012) 1640–1644.
[21] Y.S. Choi, et al., Fully implantable and bioresorbable cardiac pacemakers without leads or batteries, Nature Biotechnology 39 (10) (2021) 1228–1238.
[22] Y. Li, et al., Biodegradable, transparent, and antibacterial alginate-based triboelectric nanogenerator for energy harvesting and tactile sensing, Chemical Engineering Journal 468 (2023).
[23] C. Gao, et al., Degradable Triboelectric Nanogenerators Based on Chitosan Fibers for Smart Sensing, ACS Applied Electronic Materials 5 (7) (2023) 3865–3874.
[24] S.Y. Chao, et al., Triboelectric nanogenerator based on degradable materials, Ecomat 3 (1) (2021).
[25] J. Chen, et al., Toward Large-Scale Energy Harvesting by a UV-Curable Organic-Coating-Based Triboelectric Nanogenerator, Sensors 23 (2) (2023).
[26] L.M. Zhao, et al., A size-unlimited surface microstructure modification method for achieving high performance triboelectric nanogenerator, Nano Energy 28 (2016) 172–178.
[27] Y.J. Ma, et al., Microbial biofilms for self-powered noncontact sensing, Biosensors & Bioelectronics 247 (2024).
[28] C. Li, et al., Molecular Doped Biodegradable Triboelectric Nanogenerator with Optimal Output Performance, Advanced Functional Materials n/a(n/a) (2024) 2400277.
[29] R. Tao, et al., Integrating all-yarn-based triboelectric nanogenerator/supercapacitor for energy harvesting, storage and sensing, Chemical Engineering Journal 496 (2024).
[30] Y. Xu, et al., Technological roles of microorganisms in fish fermentation: a review, Critical Reviews in Food Science and Nutrition 61 (6) (2021) 1000–1012.
[31] T. Hu, S. Shi, Q. Ma, *Modulation effects of microorganisms on tea in fermentation.* Frontiers, Nutrition 9 (2022).
[32] Y. Song, et al., Biopharmaceutical applications of microbial polysaccharides as materials: A Review, International Journal of Biological Macromolecules 239 (2023) 124259.
[33] Sharma, C., A. Osmolovskiy, and R. Singh *Microbial Fibrinolytic Enzymes as Anti-Thrombotics: Production, Characterisation and Prodigious Biopharmaceutical Applications.* Pharmaceutics, 2021. **13**, DOI: 10.3390/pharmaceutics13111880.
[34] H. Rafeeq, et al., Genetically engineered microorganisms for environmental remediation, Chemosphere 310 (2023) 136751.
[35] V. Kugarajah, et al., Significance of microbial genome in environmental remediation, Microbiological Research 271 (2023) 127360.
[36] J.Z. Sun, et al., Microbial fuel cell-based biosensors for environmental monitoring: a review, Water Science and Technology 71 (6) (2015) 801–809.
[37] K. Saravanakumar, R. Rajeswari, Microbial fuel cell-based self-powered biosensor for environment monitoring in IoT cloud framework, Concurrency and Computation-Practice & Experience 31 (15) (2019).
[38] X.M. Liu, et al., *Microbial biofilms for electricity generation from water evaporation and power to wearables.* Nature, Communications 13 (1) (2022).
[39] Y.J. Yun, et al., Metal/bacteria cellulose nanofiber bilayer membranes for high-performance hydrovoltaic electric power generation, Nano Energy 118 (2023) 108934.
[40] Q.C. Hu, et al., *Water evaporation-induced electricity with biofilms.* Science, Advances 8 (15) (2022).
[41] E.N. Hayta, et al., Bacterial Materials: Applications of Natural and Modified Biofilms, Advanced Materials Interfaces 8 (21) (2021) 2101024.
[42] H. Yu, et al., Bacterial cellulose nanofiber triboelectric nanogenerator based on dielectric particles hybridized system, Composites Part a: Applied Science and Manufacturing 151 (2021) 106646.
[43] C. Luo, et al., Improving the Output Performance of Bacterial Cellulose-Based Triboelectric Nanogenerators by Modulating the Surface Potential in a Simple Method, ACS Sustainable Chemistry & Engineering 10 (39) (2022) 13050–13058.
[44] S. Jakmuangpak, et al., Engineering Bacterial Cellulose Films by Nanocomposite Approach and Surface Modification for Biocompatible Triboelectric Nanogenerator, ACS Applied Electronic Materials 2 (8) (2020) 2498–2506.
[45] L. He, Germination, et al., Outgrowth, and Vegetative-Growth Kinetics of Dry-Heat-Treated Individual Spores of Species, Applied and Environmental Microbiology 84 (7) (2018).
[46] Z. Li, et al., Nanogenerator-Based Self-Powered Sensors for Wearable and Implantable Electronics, Research 8710686 (2020).
[47] Y. Zou, J. Xu, K. Chen, et al., Advances in nanostructures for high-performance triboelectric nanogenerators[J], Advanced Materials Technologies 6 (3) (2021) 2000916.
[48] S. Chen, et al., Flexible and transparent sensors with hierarchically micro-nano texture for touchless sensing and controlling, Nano Energy 82 (2021) 105719.